AFRL-AFOSR-JP-TR-2018-0013

Synthesis of Electrically Conducting Polyimides for Flexible Electronic Devices

Youngkyoo Kim
Kyungpook National University

12/08/2017
Final Report

Air Force Research Laboratory
AF Office Of Scientific Research (AFOSR)/ IOA
Arlington, Virginia 22203
Air Force Materiel Command

REPORT DOCUMENTATION PAGE

Form Approved
OMB No. 0704-0188

1. REPORT DATE *(DD-MM-YYYY)*	2. REPORT TYPE	3. DATES COVERED *(From - To)*
21-02-2018	Final	12 Sep 2016 to 11 Sep 2017

4. TITLE AND SUBTITLE
Synthesis of Electrically Conducting Polyimides for Flexible Electronic Devices

5a. CONTRACT NUMBER

5b. GRANT NUMBER
FA2386-16-1-4074

5c. PROGRAM ELEMENT NUMBER
61102F

6. AUTHOR(S)
Youngkyoo Kim

5d. PROJECT NUMBER

5e. TASK NUMBER

5f. WORK UNIT NUMBER

7. PERFORMING ORGANIZATION NAME(S) AND ADDRESS(ES)
Kyungpook National University
1370 SANGYUCK-DONG BUK-GU
TAEGU, 702701 KR

8. PERFORMING ORGANIZATION REPORT NUMBER

9. SPONSORING/MONITORING AGENCY NAME(S) AND ADDRESS(ES)
AOARD
UNIT 45002
APO AP 96338-5002

10. SPONSOR/MONITOR'S ACRONYM(S)
AFRL/AFOSR IOA

11. SPONSOR/MONITOR'S REPORT NUMBER(S)
AFRL-AFOSR-JP-TR-2018-0013

12. DISTRIBUTION/AVAILABILITY STATEMENT
A DISTRIBUTION UNLIMITED: PB Public Release

13. SUPPLEMENTARY NOTES

14. ABSTRACT
The PI was successful the year long project. The PI and researchers were able to create a new synthesis method and characterize three different diamino compounds from their intermediate dinitro compounds. The PI was able to successfully characterize the new compounds with optical absorption spectroscopy and photoelectron yield spectroscopy. The compounds were then doped with acids. The doped diamino compounds were also characterized. These doped polyimides polymers can be further applied for various kinds of electronic devices through tailoring of their chemical structures in the backbones.

15. SUBJECT TERMS
Conductive Polyimides, Flexible Electronics, Polymers, Polythiophenes, Structure/Property Relationships, Synthesis

16. SECURITY CLASSIFICATION OF:			17. LIMITATION OF ABSTRACT	18. NUMBER OF PAGES	19a. NAME OF RESPONSIBLE PERSON
a. REPORT	b. ABSTRACT	c. THIS PAGE			CHEN, JERMONT
Unclassified	Unclassified	Unclassified	SAR	19	19b. TELEPHONE NUMBER *(Include area code)* 315-227-7007

Standard Form 298 (Rev. 8/98)
Prescribed by ANSI Std. Z39.18

Final Report

Title:

Synthesis of Electrically Conducting Polyimides for Flexible Electronic Devices

Principal Investigator: Prof. Youngkyoo Kim

Organic Nanoelectronics Laboratory (ONELAB), Department of Chemical Engineering, Division of Applied Chemical Engineering, Kyungpook National University, University Road 80, Daegu 41566, Republic of Korea
(E-mail: ykimm@knu.ac.kr)

Key Researchers: Dr. Hwajeong Kim

Organic Nanoelectronics Laboratory (ONELAB), Department of Chemical Engineering, Division of Applied Chemical Engineering, Kyungpook National University, University Road 80, Daegu 41566, Republic of Korea
(E-mail: khj217@knu.ac.kr)

Mr. Joonwoo Kim

Organic Nanoelectronics Laboratory (ONELAB), Department of Chemical Engineering, Division of Applied Chemical Engineering, Kyungpook National University, University Road 80, Daegu 41566, Republic of Korea
(E-mail: kjw12n@lycos.co.kr)

Mr. Euiyoung Park

Organic Nanoelectronics Laboratory (ONELAB), Department of Chemical Engineering, Division of Applied Chemical Engineering, Kyungpook National University, University Road 80, Daegu 41566, Republic of Korea
(E-mail: kalindus@naver.com)

Period-of-Performance: 1 Year (2016/10/01 – 2017/09/30)

Total Cost: $45,000

Abstract:

A remarkable paradigm change is in progress from rigid electronics to flexible electronics featuring flexible, ultrathin and lightweight devices. To achieve real flexible electronics, it is understood that electrodes should be made with plastics (polymers) instead of conventional rigid and brittle inorganic materials. Although various conducting polymers have been developed to date, they failed to be widespread because of their fundamental disadvantages including low durability (easy tear) and poor processability. Here we propose "***conducting polyimides (CPIs)***" because polyimides are well known for their excellent mechanical/thermal stability as well as good processablility. In this work, as one of the pioneering steps, three types of CPIs have been developed via stepwise synthesis from corresponding three types of dinitro compounds. The resulting diamino compounds (B-type, Q-type and T-type), which were synthesized via reduction reaction from the dinitro compounds, were polymerized with pyromellitic dianhydride leading to poly(amic acid)s (PAAs). The soluble PAA polymers were chemically doped using organosulfonic acids including p-toluenesulfonic acid, leading to the doped PI films. The resulting doped PI films exhibited good electrical conductivity comparable to the conventional conducting polymers (PEDOT:PSS). When the doped Q-type PI polymers were used as an electron-collecting hybrid buffer layer for the inverted-type organic solar cells, the performance of solar cells was comparable to the reference solar cells.

INTRODUCTION

A drastic paradigm change is in progress from rigid electronics to flexible electronics. In addition to flexibility, ultrathin and lightweight features are being mandatory for recent electronic devices [1-3]. To achieve real flexible electronics, the electrodes in devices should be made with plastics (polymers) instead of conventional rigid and brittle inorganic materials [4-6]. Although various conducting polymers have been developed to date, they failed to be widespread because of their fundamental disadvantages including low durability (easy tear) and poor processability [7-10]. It has been also reported that graphenes also suffer from the intrinsic limitation of processability owing to the restricted number of layers, only one layer theoretically, for securing flexibility [11-13].

Polyimides (PIs) are known to possess outstanding film-forming and physically durable characteristics so that they have been used as one of the representative electrically insulating materials for microelectronic industries [14,15]. The insulating polyimides have been attempted to apply as a host for hole injection and/or transport layers in organic light-emitting devices (OLEDs) [16-19]. However, the intrinsic nature of such insulating polyimides could not further improve the performance of OLEDs. In 1999, it has been reported that polyimides can possess semiconducting properties by incorporating a semiconducting unit into the polyimide backbones [20-22]. However, the semiconducting polyimides require sufficient external voltages to function properly, which limited their applications for other devices. This motivated us to develop conducting polyimides (CPIs) as illustrated in Fig. 1.

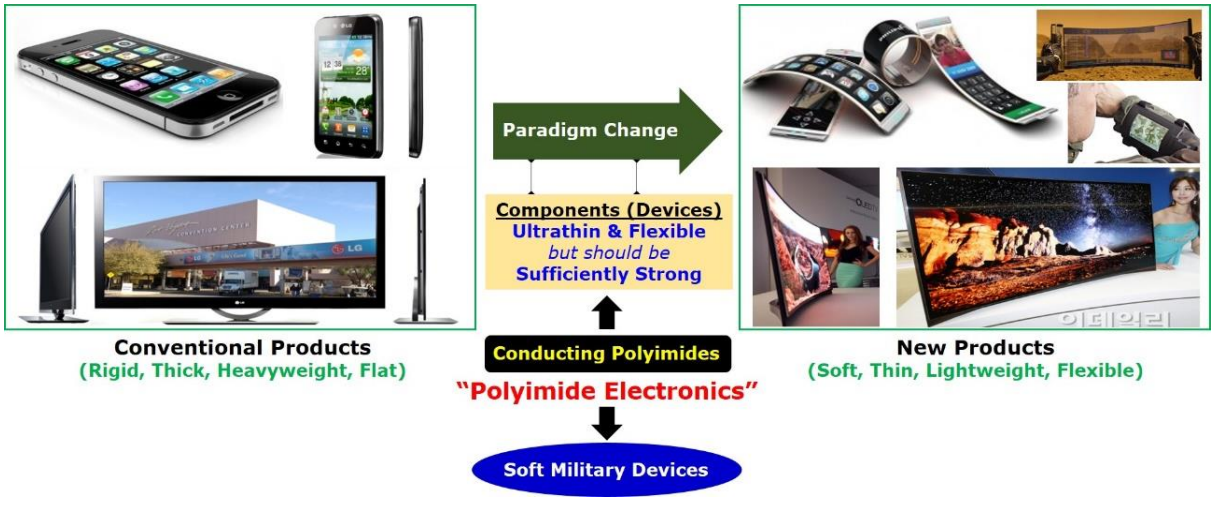

Figure 1. Illustration for the reason why conducting polyimides (CPIs) are required and creation of "polyimide electronics" fields.

In this report, we demonstrate that semiconducting polyimides (CPIs) can be electrically conductive via chemical doping processes leading to a charged state in the polyimide backbones. In order to prove this idea, semiconducting polyimides (SPIs) have been synthesized by polymerization of dianhydrides

and diamines that were newly synthesized for this project. Results showed that the energy band structure of the synthesized semiconducting polyimides was dependent on the type of core building blocks in three different diamine compounds. The chemical doping delivered a noticeable shift in the highest occupied molecular orbital (HOMO) energy level for the three polyimides synthesized in this work. In particular, the electrical conductivity of the present polyimides was significantly enhanced by the chemical doping. As a consequence, the present doped polyimides could act as an electron-collecting buffer layer in inverted-type organic solar cells with the bulk heterojunction active layers [23-28].

METHODS

Synthesis of B-type Dinitro and Diamine Compounds

Three different dinitro compounds were synthesized by employing either Stille and Suzuki coupling reactions. The B-type dinitro compound was synthesized by reacting between 2-bromo-5-nitrothiophene and bis(4,4,5,5-tetramethyl-1,3,2-dioxaborolan-2-yl)-X,Y-benzene in the presence of tetrakis(triphenylphosphine)palladium (0) ($Pd(Ph_3)_4$) and potassium carbonate (K_2CO_3). The coupling reaction was carried out for ca. at 70 ^oC. After terminating the reaction, the reacted solutions were precipitated in methanol, followed by repeated washing in order to purify. The synthesis yield was 84.5%. The B-type dinitro compound synthesized was added to the mixture solutions of tetrahydrofuran and deionized water including ammonium chloride (NH_4Cl,) and zinc (Zn). These mixture solutions were subjected to the reduction reaction over 24 h, which led to corresponding B-type diamino compound with a violet color. The reduction yield was ca. 82%. The B-type dinitro and diamino compounds were characterized with mass spectrometer and nuclear magnetic resonance spectrometer (^{1}H-NMR and ^{13}C-NMR).

Synthesis of Q-type Dinitro and Diamine Compounds

The Q-type dinitro compound was synthesized by the reaction of 2-bromo-5-nitrothiophene and bis(trimethylstannyl)-3,3'-W-heterocycle in the presence of tetrakis(triphenylphosphine)palladium (0) ($Pd(Ph_3)_4$). The starting solutions were continuously stirred under nitrogen atmosphere for more than 24 h at ~70 ^oC. Then the reacted solutions were cooled down slowly, followed by making precipitates using methanol. The precipitates were filtrated using a filter paper and subjected to the sequential purification process. Finally, a black solid (Q-type dinitro compound) was obtained with the synthesis yield of 77.2% after drying in a vacuum oven. The similar reduction reaction as done for the B-type dinitro compound was performed to reduce the Q-type dintro compound to corresponding Q-type diamino compound. The reduction yield from the Q-type dintro compound to the Q-type diamino compound was ca. 85%. The Q-type dinitro and diamino compounds after purification were

characterized using mass spectrometer and nuclear magnetic resonance spectrometer (^{1}H-NMR and ^{13}C-NMR).

Synthesis of T-type Dinitro and Diamine Compounds

To synthesize the T-type dinitro compound, bis(trimethylstannyl)-Z-biheterocycle was reacted with 2-bromo-5-nitrothiophene in the presence of tetrakis(triphenylphosphine)palladium (0) ($Pd(Ph_3)_4$). The reaction was over 24 h, while the temperature was kept at around 70 ^{o}C. After finishing the coupling reaction, the solutions were cooled down to room temperature. To separate the T-type dinitro compound from catalysts, methanol was slowly added to the final solutions. The precipitates obtained were purified through repeated filtration steps. Finally, the T-type dinitro compound with a black color was obtained after drying in vacuum. The final synthesis yield was 80.3%. Next, the T-type dinitro compound was converted to corresponding T-type diamino compound by employing the same reduction reaction as done for the Q-type dinitro compound. The reduction yield of the T-type diamino compound (brown color) was ca. 78%. Both Q-type dinitro and diamino compounds were subjected to characterization using mass spectrometer and nuclear magnetic resonance spectrometer (^{1}H-NMR and ^{13}C-NMR).

Synthesis of Poly(amic acid)s

The three different diamino compounds synthesized above were individually reacted with pyromellitic dianhydride (PMDA), which led to individual poly(amic acid) (PAA). Frist, the B-type diamino compound was dissolved in dimethyl acetamide (DMAc), which was added to the solution including PMDA. The polymerization reaction was carried out at around 0 ^{o}C by controlling the reaction time between 3 h and 72 h. After terminating the reaction, the product PAA was solidified by pouring the solutions into excess methanol. Finally, the reddish solid product was dried in a vacuum oven at room temperature. The polymerization yield was 93%. The similar polymerization process was applied for the rest two (Q-type and T-type) diamino compounds. The polymerization yield was ca. 72.9% and 75.2% for Q-type PAA and T-type PAA, respectively.

Film and Device Fabrication

The PAA solutions were coated on quartz substrates for the measurement of optical absorption spectra, while indium-tin oxide (ITO)-coated glass substrates were used for other analysis including device fabrication. The PAA films coated on the substrates were thermally imidized leading to corresponding PI films for all samples. In order to fabricate devices, diodes and solar cells, the ITO-glass substrates were subjected to conventional photolithography/etching processes in order to pattern the ITO electrodes. The patterned ITO-glasses were cleaned using acetone and methanol or isopropyl alcohol,

followed by dry cleaning under UV-ozone. The diode devices were fabricated by depositing aluminum electrodes on the PI films which were converted from their PAA films coated on the patterned ITO-glass substrates. For the fabrication of organic solar cells (inverted type), first, the PAA films with or without additional metal oxides were spin-coated on the patterned ITO-glass substrates and thermally imidized at 250 ^{o}C. Next, the active layers, which consist of poly[4,8-bis(5-(2-ethylhexyl)thiophen-2-yl)benzo[1,2-b:4,5-b0]dithiophene-alt-3-fluorothieno[3,4-b]thiophene-2-carboxylate] (PTB7-Th) and [6,6]-phenyl-C71-butyric acid methyl ester ($PC_{71}BM$), were spin-coated on the PI layers. Finally, molybdenum oxide (MoO_3, 10 nm) and silver (Ag, 80 nm) were sequentially deposited on the active layers. The thickness of the PI (hybrid) layers was varied between 0 nm and 100 nm for the examination of diode-type devices and organic solar cells.

Measurement and Analysis

The thickness of the PAA and PI films was measured using a surface profilometer (Alpha Step 200, Tencor Instruments). The optical absorption and photoelectron (PE) yield spectra of films were measured using a UV-visible-near infrared spectrometer (Lambda 750, Perkin Elmer) and a PE spectrometer (AC-2, Hitachi High Tech), respectively. The current density – voltage (J-V) characteristics of devices were measured using an electrometer (Model 2400, Keithley), while the solar cell performances were measured using a solar simulator (92250A-1000, Newport-Oriel). The dinitro and diamino compounds were characterized using a gas chromatography-mass spectrometer (7890B-5977B GC/MSD, Agilent) and a nuclear magnetic resonance spectrometer (AVANCE III 500, Bruker). The viscosity of the PAA solutions was examined by employing a viscometer.

RESULTS AND DISCUSSION

As shown in Fig. 2, three different dinitro compounds (**5**: B-type, **6**: Q-type, **7**: T-type) were successfully synthesized via Stille or Suzuki coupling reactions. Then the dinitro compounds were converted to corresponding diamino compounds through the reduction reaction by employing the mixed catalyst systems (see the method section). The resulting diamine compounds showed different colors: maroon (**8**, B-type), black (**9**, Q-type), and dark green (**10**, T-type). As explained in the method section, the average synthesis yield was more than 77 % for the dinitro compounds and 85 % for the diamino compounds.

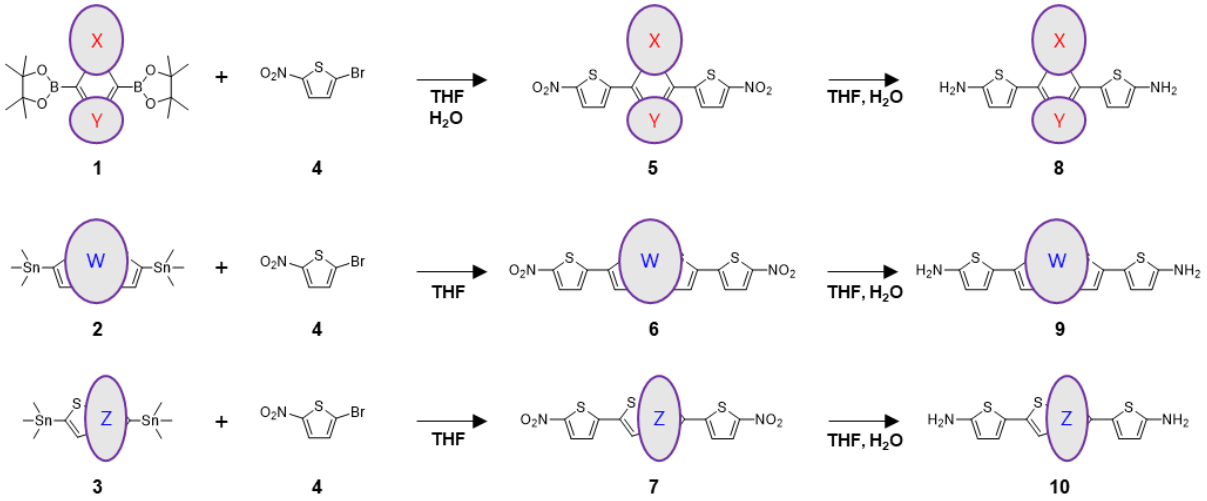

Figure 2. Synthesis of three different dinitro compounds (**5**: B-type, **6**: Q-type, **7**: T-type) via Stille or Suzuki coupling reactions of bi-functional compounds (**1**~**3**) with 4-bromo-4'-nitrothiophene (**4**). The diamino compounds (**8**: B-type, **9**: Q-type, **10**: T-type) were synthesized by reduction process from corresponding dinitro compounds. Note that the backbones (B-type, Q-type, T-type) are different according to the constituents, 'X', 'Y', 'W', and 'Z', which consist of mixed structures including phenyl groups and alkylated heterocycles.

Next, as depicted in Fig. 3, the diamino compounds (**8**~**10**) were reacted with pyromellitic dianhydride (PMDA, **11**) at a low temperature (ca. 0 °C), which led to corresponding poly(amic acid) (PAA) precursors (**12**~**14**). In order to increase both reactivity and yield, various attempts have been tried by varying reaction time and stirring conditions. The color of PAA precursors was red (**12**), yellowish brown (**13**), and brown (**14**). The solutions of PAA precursors were subjected to precipitation in methanol for characterizations and applications for devices. To prepare thin PAA films, the PAA solutions were spin-coated on glass or quartz substrates. After soft-baking, these PAA films were thermally imidized at 250 °C for ca. 2 h, which resulted in corresponding polyimide (PI) films. The thermal imidization processes changed the film color to purple (**15**), dark brown (**16**), and light brown (**17**).

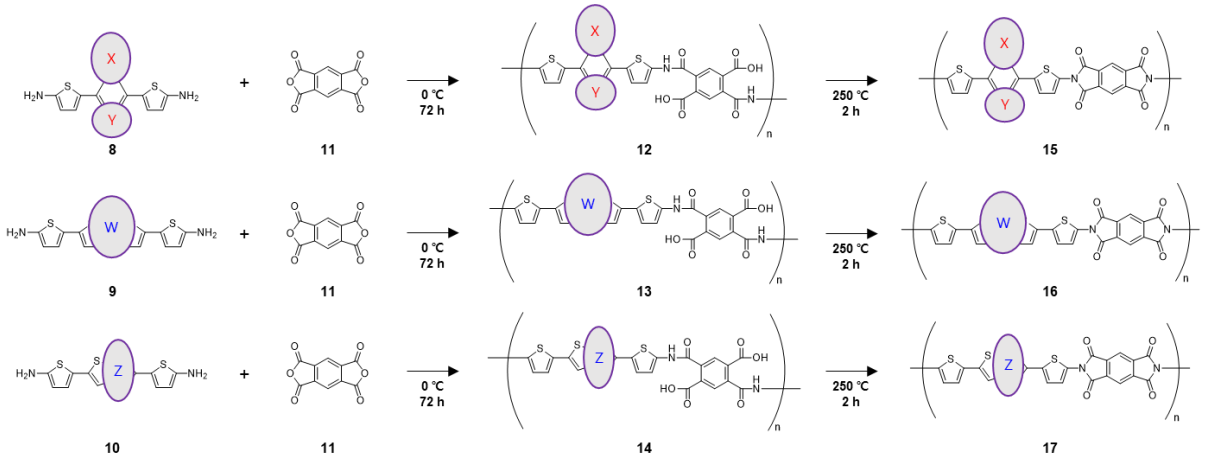

Figure 3. Polymerization of PAA precursors (**12**: B-type, **13**: Q-type, **14**: T-type) from three different diamino compounds (**8**~**10**) and PMDA (**11**). The PAA precursor polymers were converted to corresponding PI polymers (**15**: B-type, **16**: Q-type, **17**: T-type) via thermal imidization process. Note that the backbones (B-type, Q-type, T-type) are different according to the constituents, 'X', 'Y', 'W', and 'Z', which consist of mixed structures including phenyl groups and alkylated heterocycles.

The dinitro compounds (**5**~**7**) synthesized above were characterized with optical absorption spectroscopy and photoelectron yield spectroscopy. As shown in Fig. 4a, the maximum peak of absorption spectra was different for the three dinitro compounds. The T-type dinitro compound exhibited the shortest wavelength for the maximum absorption peak, while the similar position was measured for both the Q-type and T-type dinitro compounds. Looking into the absorption edges (see the inset in Fig. 4), the onset point of optical absorption was considerably different with respect to the type of dinitro compounds. These onset points deliver the optical band gap energy of 5.55 eV for the B-type dinitro compound, 5.2 eV for the Q-type dinitro compound, and 5.25 eV for the T-type dinitro compound. In addition to the optical band gap energy, the highest occupied molecular orbital (HOMO) energy level of the present dinitro compounds was obtained from the photoelectron yield spectra in Fig. 4b. As pointed by the arrows, the HOMO energy level was 5.72 eV for the B-type dinitro compound, 5.68 eV for the Q-type dinitro compound, and 4.73 eV for the T-type dinitro compound.

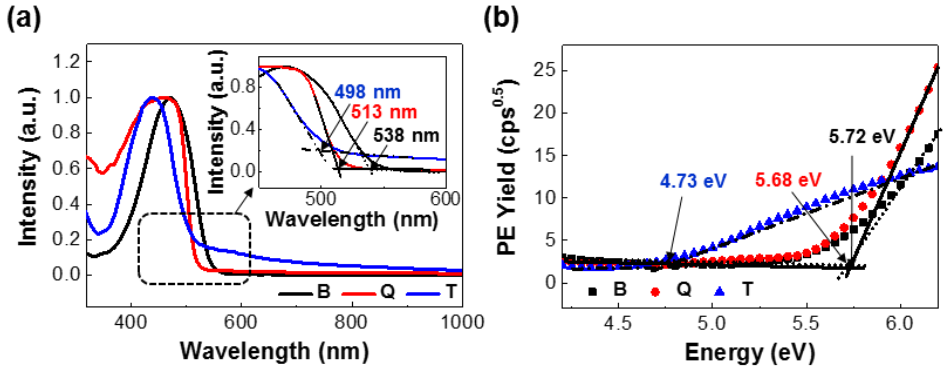

Figure 4. Characterization of optical absorption and electronic structures for the dinitro compounds (B: B-type, Q: Q-type, T: T-type) synthesized in this work: (a) optical absorption spectra (inset: absorption edges), (b) photoelectron yield spectra (see the HOMO energy value marked by arrows).

The diamino compounds (**8**~**10**) synthesized above were also characterized with optical absorption spectroscopy and photoelectron yield spectroscopy. As shown in Fig. 5a, the absorption spectral shape of the diamino compounds was certainly different according to the type of diamino compounds. The B-type diamino compound showed pronounced double absorption peaks, while the T-type diamino compound had a shoulder peak at around 550 nm. In contrast, only single absorption peak was measured for the Q-type diamino compound. The photoelectron yield spectra disclosed that the HOMO energy level was 5.68 eV for the B-type diamino compound, 5.51 eV for the Q-type diamino compound, and 5.47 eV for the T-type diamino compound. Therefore, it is shortly concluded that the HOMO energy level of the diamino compounds could be very close after reduction reaction, even though the HOMO energy level of the dinitro compounds was different according to the type of core building units.

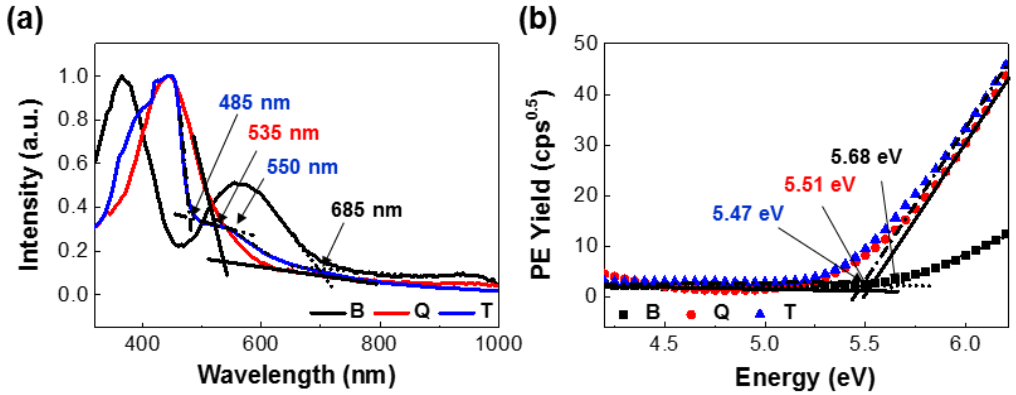

Figure 5. Characterization of optical absorption and electronic structures for the diamino compounds (B: B-type, Q: Q-type, T: T-type): (a) optical absorption spectra (see characteristic absorption edges marked by arrows), (b) photoelectron yield spectra (see the HOMO energy value marked by arrows).

The same optical absorption spectroscopy and photoelectron yield spectroscopy measurements were applied to characterize the PI films. As shown in Fig. 6a, the spectral shape was almost similar for the Q-type and T-type PI films. However, the B-type PI films exhibited a double absorption shape, which can be attributable to the double absorption shape of corresponding PAA films (see Fig. 5a). As indicated by arrows in the inset graph, the absorption edge was different with respect to the type of core building blocks in the diamine units. The T-type PI films showed the longest absorption edge up to 591 nm. The photoelectron yield spectra in Fig. 6b disclosed that the HOMO energy level of the present PI films is in the range of 5.4~5.63 eV, which is marginally shifted from that of the diamino compounds.

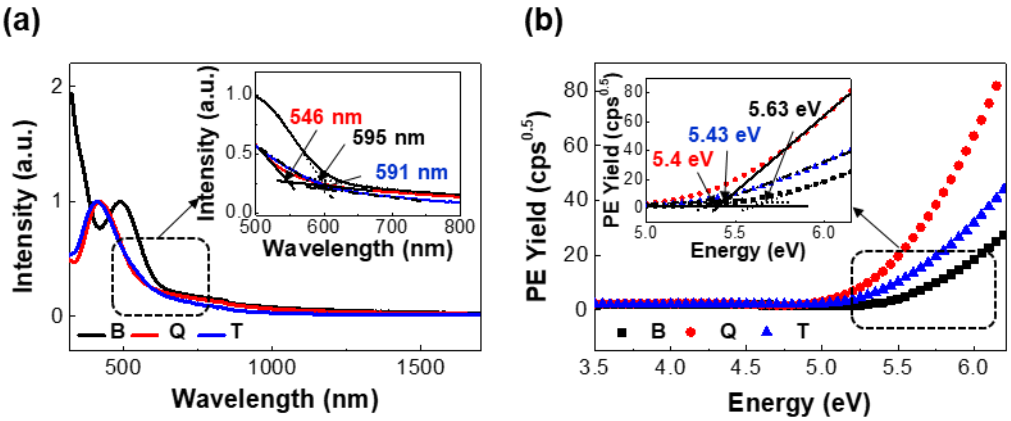

Figure 6. Characterization of optical absorption and electronic structures for the PI films (B: B-type, Q: Q-type, T: T-type): (a) optical absorption spectra (see characteristic absorption edges marked by arrows), (b) photoelectron yield spectra (see the HOMO energy value marked by arrows).

Based on the characterization results for the materials synthesized, the possibility of chemical doping was investigated by varying the kind of acidic dopants such as p-toluenesulfonic acid (TSA), ethylbenzenesulfonic acid (EBSA), etc. As demonstrated as an example in Fig. 7a, the color of PAA powders was obviously changed to deep green when dopants were dropped to the solid samples. In order to further examine the capability of doping directly to the films, the dopants were applied to both PAA and PI films. As observed from the photographs in Fig. 7b, the color of the PAA films was clearly changed (see the dropped regions) irrespective of the type of core building blocks. However, the PI films were less reactive to the dopants than the PAA films, which can be explained by the high chain stacking structures after thermal imidization.

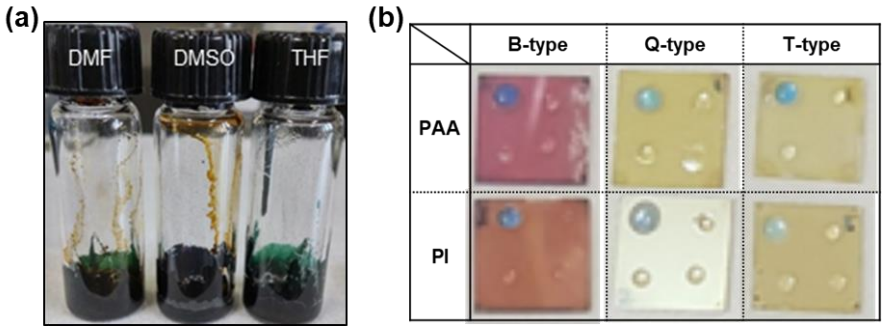

Figure 7. Doping test results for the PAA powders and films (PAA and PI): (a) Green color after doping for the PAA powders according to the different kind of solvents used, (b) Color change for the PAA and PI films by dopants according to the type of core building blocks.

Considering the color change by applying dopants to the PAA and PI films (see Fig. 7b), the possible doping mechanism was built as shown in Fig. 8. In principle, the dopant molecules might approach toward the functional building block units, which have sufficient electrons liable, upon mixing. Then the doping process could be happened, whether the dopant molecules are strongly bound to the electron-donating parts of core building blocks or not, by making a complex doped state. After thermal imidization, the doped state could be still reserved even though some dopant molecules could be removed by thermal activation. As a consequence, the doped PI films can have a partially charged state due to the presence of dopant molecules, which is expected to deliver electrical conductivity in the present PI films.

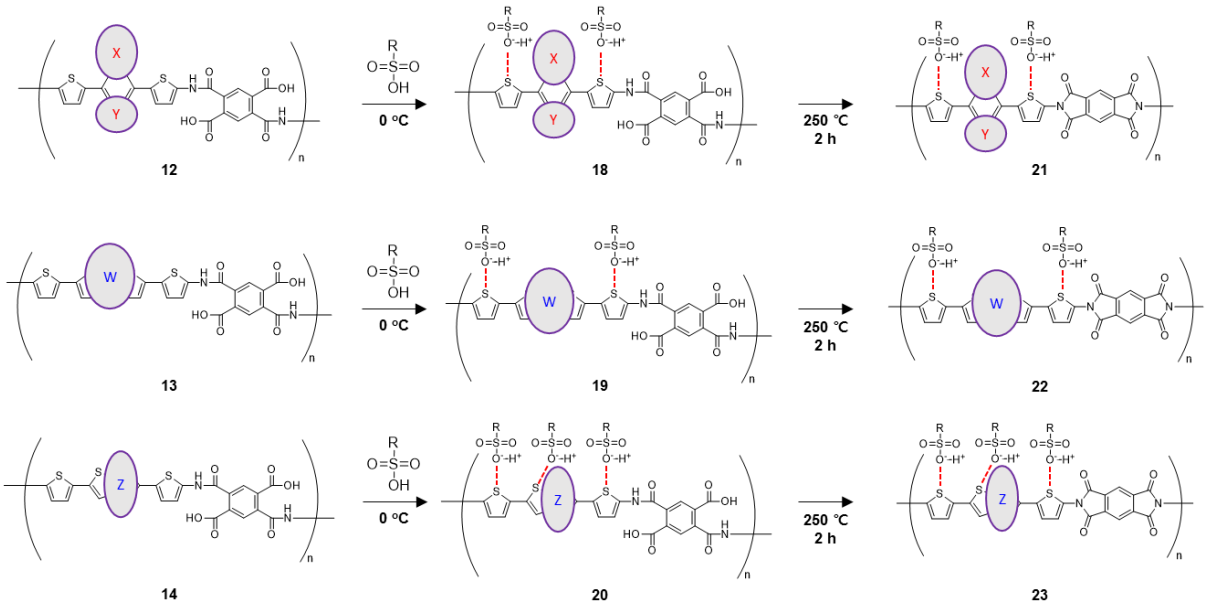

Figure 8. A simplified doping mechanism for the PAA and PI films. The 'R' group in the dopant molecule represent hydrogen, methyl, toluene, ethylbenzene, etc. The thermal imidization temperature can be adjusted according to the type of dopants, while the imdization yield may be varied with the conditions.

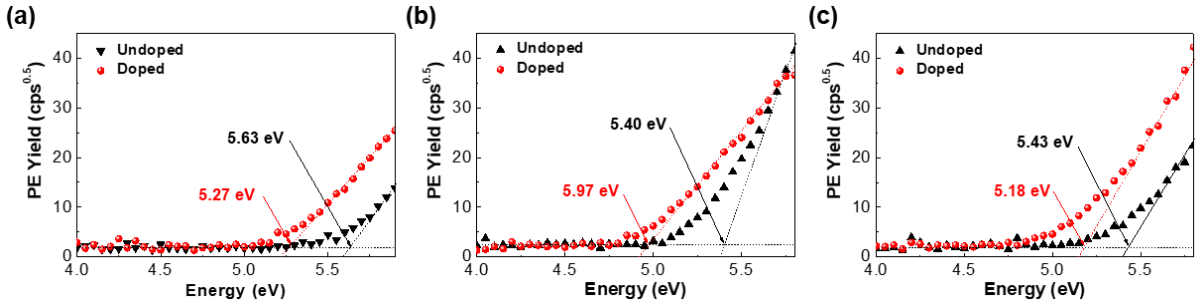

Figure 9. Photoelectron yield spectra for the PI films before and after doping: (a) B-type PI, (b) Q-type PI, and (c) T-type PI. The onset point corresponding to the HOMO energy level is marked by arrows. Note that the HOMO energy level was shifted by doping for all the PI films irrespective of the type of core building blocks.

The HOMO energy level of the doped PI films was investigated with photoelectron yield spectroscopy. As shown in Fig. 9, the HOMO energy level of the PI films was shifted to the lower energy region without respect to the type of core building blocks. The degree of onset point shift was 0.36 eV for the B-type PI film, 0.43 eV for the Q-type PI film, and 0.25 eV for the T-type PI film. The smallest onset point shift was measured for the T-type PI film after doping. This result supports that the doping in the PI films is considerably dependent on the type of core building blocks. The reason on the shift in the HOMO energy level can be ascribed to the change in the density of state (HOMO level) by the interaction of dopant molecules.

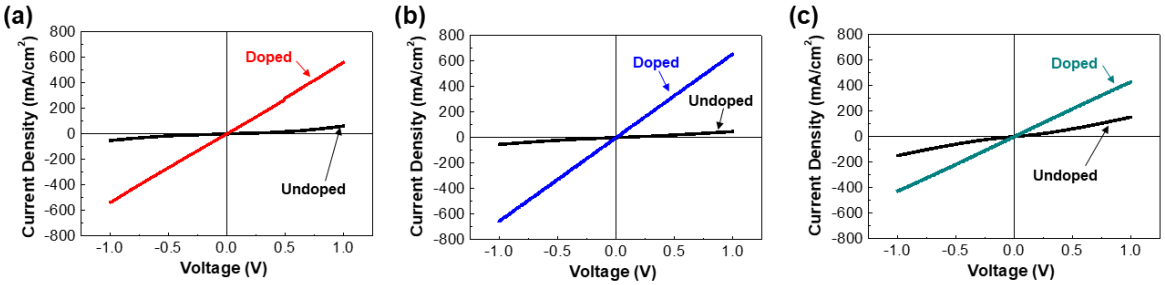

Figure 10. Current density – voltage (J-V) characteristics of PI films in the diode type device geometry (glass/ITO/PI/Al): (a) B-type PI, (b) Q-type PI, and (c) T-type PI. The thickness of each PI film was 50 nm.

Next, the electrical conductivity of the PI films was measured in order to examine the doping effect by employing the diode type device structure (parallel plate geometry). As shown in Fig. 10a, the shape of current density – voltage (J-V) curves was an inversed sigmoidal shape for the B-type PI films before doping. This result reflects that the undoped PI films follow semiconducting characteristics. However, the doped B-type PI films exhibited a straight line that represents an ohmic behavior. In addition, the

current density of the B-type PI films was significantly enhanced after doping, which supports the increased electrical conductivity.

Table 1. Summary of electrical resistivity and conductivity for the three different PI films which were measured by employing a diode type device geometry (glass/ITO/PI/Al). Note that the electrical resistivity and conductivity were 4.65×10^{5} Ω·cm and 2.15×10^{-6} S/cm for the PEDOT:PSS films (a representative conducting polymer) (see *Organic Electronics*, **2013**, 14, 2889).

Doped PI Films	Resistivity (Ω·cm)	Conductivity (S/cm)
B-type	$\mathbf{3.65\times10^{5}}$	$\mathbf{2.74\times10^{-6}}$
Q-type	$\mathbf{3.05\times10^{5}}$	$\mathbf{3.27\times10^{-6}}$
T-type	$\mathbf{4.68\times10^{5}}$	$\mathbf{2.14\times10^{-6}}$

The Q-type PI films showed the similar trend as for the B-type PI films but the current density was slightly higher at the same thickness condition (see Fig. 10b). However, it was measured that the current density of the T-type PI films before doping became already higher than that of the other undoped PI films, indicative of better metallic characteristics (see Fig. 10c). Interestingly, the doped T-type PI films showed relatively lower current density than the B-type and Q-type PI films. From the J-V curves, both electrical resistivity and conductivity were calculated as summarized in Table 1. The highest electrical conductivity (3.27×10^{-6} S/cm) was obtained from the Q-type PI films. Here it is worthy to note that the electrical conductivity of PEDOT:PSS, a well-known conducting polymer, exhibited 2.15×10^{-6} S/cm in the case of the same device geometry. This result indicates that the present PI films after doping have very competitive electrical conductivity to conventional conducting polymers.

In order to examine the performance of the present doped PI films, organic solar cells with an inverted type structure were fabricated as depicted in Fig. 11. The doped PI films were designed to collect electrons from the active layers in the devices. As shown in Fig. 12, the refence device delivered the power conversion efficiency (PCE) of 6.27% in the present device structure. Interestingly, the devices with the doped PI films exhibited good solar cell performances. The PCE of devices reached 5.68% and 6.28% in the case of the Q-type and T-type PI films. This result indicates that the performance of solar cells could be marginally improved by the T-type PI films, not by the Q-type PI films.

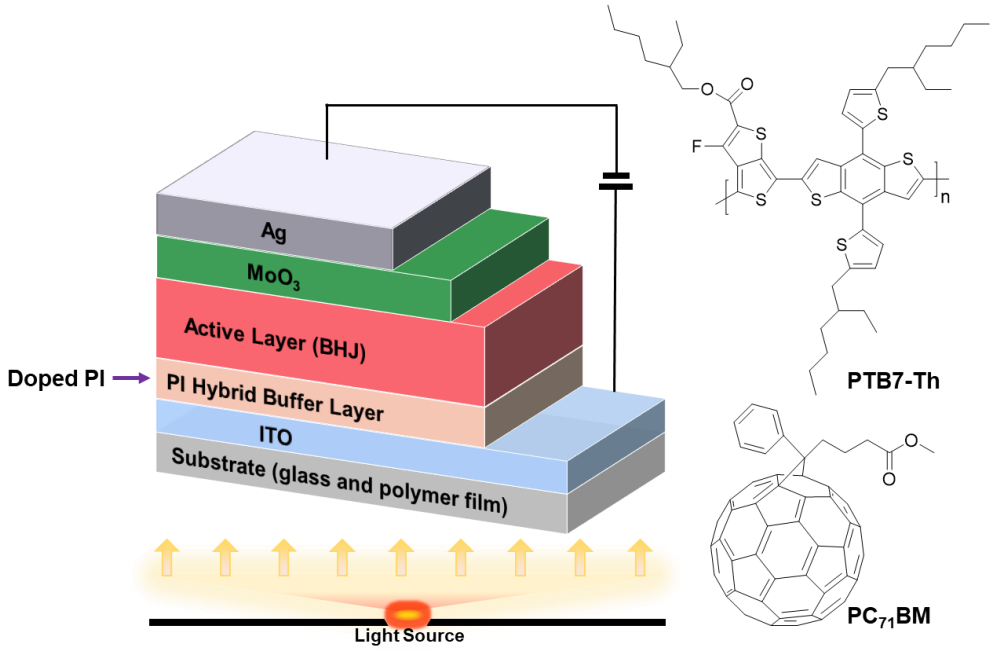

Figure 11. Illustration for the inverted-type organic solar cells with the bulk heterojunction layers of PTB7-Th and $PC_{71}BM$. The doped PI films were applied as an electron-collecting buffer layer, which has been typically prepared with ZnO films.

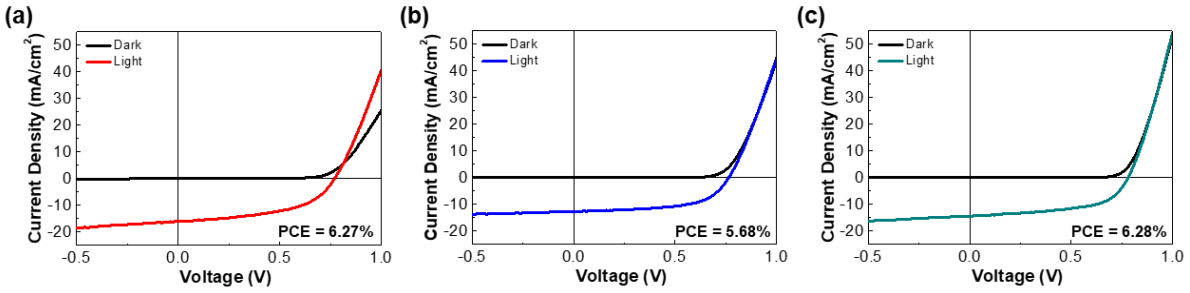

Figure 12. Current density – voltage (J-V) characteristics for the inverted-type PTB7-Th:$PC_{71}BM$ solar cells with three different electron-collecting (hybrid) buffer layers: (a) reference (ZnO), (b) Q-type PI, and (c) T-type PI. The light J-V curves were measured under illumination with a simulated solar light (100 mW/cm^2, air mass 1.5G).

Finally, the maximum power density (P_M), which can be provided from the present solar cells, was calculated from the light J-V curves in Fig. 12. As shown in Fig. 13, the doped T-type PI films could deliver the similar maxim power density as the reference cells can provide. However, the maximum power density from the solar cells with the doped Q-type PI films was as low as by 5.7 mW/cm^2 compared to the reference solar cells. This result supports that the present doped PI films can be applied for high efficiency organic solar cells by further optimization.

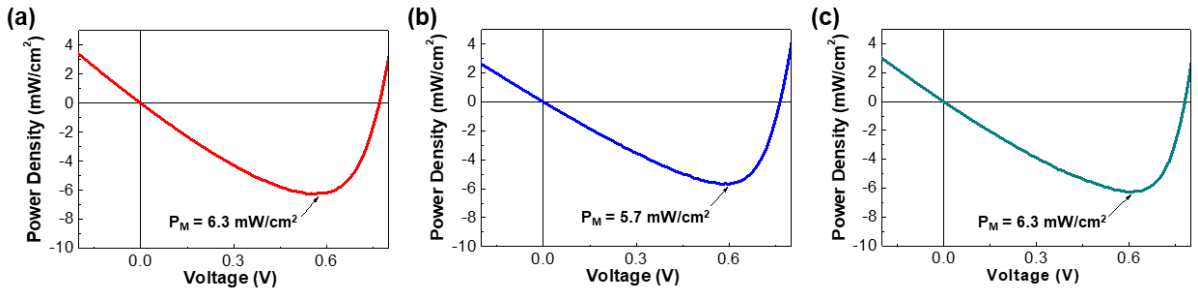

Figure 13. Power density – voltage characteristics for the inverted-type PTB7-Th:$PC_{71}BM$ solar cells with three different electron-collecting (hybrid) buffer layers: (a) reference (ZnO), (b) Q-type PI, and (c) T-type PI. The maximum power density (P_M) is given on each graph.

As summarized in Table 2, however, the short circuit current density (J_{SC}) was relatively lower for the devices with the T-type PI films than the reference case. Looking into other parameters, the fill factor (FF) was impressively higher for the doped PI films than the reference case. In addition, the shunt resistance (R_{SH}) was found additional benefit in the case of using the doped PI films.

Table 2. Summary of solar cell parameters characteristics for the inverted-type PTB7-Th:$PC_{71}BM$ solar cells with three different electron-collecting (hybrid) buffer layers.

	Reference	Q-type PI (doped)	T-type PI (doped)
V_{OC} (V)	0.77	0.76	0.78
J_{SC} (mA/cm^2)	16.0	12.7	14.4
FF (%)	50.9	58.9	55.9
PCE (%)	6.27	5.68	6.28
R_S (kΩ·cm^2)	0.16	0.16	0.13
R_{SH} (kΩ·cm^2)	1.8	3.6	3.6

CONCLUSIONS

In summary, three different diamino compounds were successfully synthesized via their intermediates (dinitro compounds) which were obtained by Stille or Suzuki coupling reactions. The B-type diamino compound showed better optical absorptions at longer wavelengths. The PAA polymers, which were individually polymerized using the three different diamino compounds and PMDA, exhibited good solubility in solvent (DMAc) as well as high solution processability. The PI films obtained by thermal imidization of the PAA films delivered slightly different HOMO energy levels (5.4 eV ~ 5.6 eV) according to the type of core building blocks in the diamine compounds. The electrical conductivity of the doped PI films was significantly enhanced by the chemical doping of corresponding PAA polymers.

The highest conductivity was obtained for the Q-type PI films, which was higher than the electrical conductivity of the well-known PEDOT:PSS films. The doped PI electron-collecting hybrid buffer layers were successfully applied for the operation of the inverted-type organic solar cells with the polymer:fullerene bulk heterojunction layers. Finally, it is expected that the present doped PI polymers can be further applied for various kinds of electronic devices through tailoring of their chemical structures in the backbones.

REFERENCES

1. M. Kaltenbrunner, M. S. White, E. D. Głowacki, T. Sekitani, T. Someya, N. S. Sariciftci and S. Bauer, *Nat. Commun.*, **3**, 770 (2012)
2. J. Lewis, *Mater. Today*, **9**, 38 (2006)
3. B. S. Ong, Y. Wu, P. Liu and S. Gardner, *J. Am. Chem. Soc.*, **126**, 3378 (2004)
4. H. Yi, M. M. Payne, J. E. Anthony and V. Podzorov, *Nat. Commun.*, **3**, 1259 (2012)
5. K. Tvingstedt and O. Inganäs, *Adv. Mater.*, **19**, 2893 (2007)
6. L. Nyholm, G. Nyström, A. Mihranyan and M. Strømme, *Adv. Mater.*, **23**, 3751 (2011)
7. J. E. Anthony, *Chem. Rev.*, **106**, 5028 (2006)
8. A. Pron, P. Gawrys, M. Zagorska, D. Djurado and R. Demadrille, *Chem. Soc. Rev.*, **39**, 2577 (2010)
9. F. Zhang, M. Johansson, M. R. Andersson, J. C. Hummelen and O. Inganas, *Adv. Mater.*, **14**, 662 (2002)
10. D. M. de Leeuw, M. M. J. Simenon, A. R. Brown, R. E. F. Einerhand, *Synth. Met.*, **87**, 53 (1997)
11. S. Nam, M. Shin, H. Kim, C.-S. Ha, M. Ree, and Y. Kim, *Adv. Funct. Mater.*, **21**, 4527 (2011).
12. H. Kim, S. Y. Kim, S. Nam, G. V. Ronnett, H. S. Han, C. Moon, and Y. Kim, *Analyst*, **137**, 2047 (2012).
13. S. Nam, Y.-G. Ko, S. G. Hahm, S. Park, J. Seo, H. Lee, H. Kim, M. Ree, and Y. Kim, NPG Asia Mater., **5**, e33 (2013).
14. D. Liaw, K. Wang, Y. Huang, K. Lee, J Lai and C. Ha, *Progress in Polymer Science*, **37**, 907 (2012)
15. F. Zhang, C. Tuck, R. Hague, Y. He, E. Saleh, Y. Li, C. Sturgess and R. Wildman, *J. Appl. Polym. Sci.*, **133**, 43361 (2016)
16. H. Lim, H. Park, J. Lee, Y. Kim, W. Cho and C. Ha, *Mol. Cryt. Liq. Cryst*., **316**, 301 (1998)
17. Y. Kim, J. Keum, J. Lee, H. Lim and C. Ha, *Adv. Mater. Opt. Electron.*, **10**, 273 (2000)
18. H. Lim, H. Park, J. Lee, Y. Kim, W. Cho and C. Ha, *SPIE*, **3281**, 345 (1998)
19. H. Park, H. Lim, Y. Kim, W. Cho and C. Ha, *Mol. Cryt. Liq. Cryst.*, ***316***, 265 (1998)
20. Y. Kim, J. Lee, K. Han, H. Hwang, D. Choi, Y. Jung, J. Keum, S. Kim, S. Park and W. Im, *Thin Solid Films.*, **363**, 263 (2000)
21. Y. Kim, K. Han and C. Ha, *Macromolecules*, **35**, 8759 (2002)
22. Y. Kim, K. Bae, Y. Jeong, D. Choi and C. Ha, *Chem. Mater.*, **16**, 5051 (2004)
23. J. Jeong, S. Woo, S. Park, H. Kim, S. Lee and Y. Kim, *Org. Electron.*, **14**, 2889 (2013)
24. S. Nam, J. Seo, S. Woo, W. H. Kim, H. Kim, D. D. Bradley and Y. Kim, *Nat. Commun.*, **6**, 8929 (2015).
25. S. Nam, J. Seo, M. Song, H. Kim, M. Ree, Y. Gal, D. D. C. Bradley and Y. Kim, *Org. Electron.*, **48**, 61 (2017)

26. H. Han, H. Lee, S. Nam, J. Jeong, I. Lee, H. Kim, C. Ha and Y. Kim, *Polym. Chem.*, **4**, 2053 (2013)
27. W. Zhao, S. Li, H. Yao, S. Zhang, Y. Zhang, B. Yang and J. Hou, *J. Am. Chem. Soc.*, **139**, 7148 (2017)
28. X. Li, X. Liu, W. Zhang, H. Wang and J. Fang, *Chem. Mater.*, **29**, 4176 (2017)
29. Z. Zheng, O. M. Awartani, B. Gautam, D. Liu, Y. Qin, W. Li, A. Bataller, K. Gundogdu, H. Ade and J. Hou, *Adv. Mater*., **29**, 1604241 (2017)